Attraction of Iodide Ions by the Free Water Surface, Revealed by Simulations with a Polarizable Force Field Based on Drude Oscillators

Georgios Archontis,*,† Epameinondas Leontidis,*,‡ and Georgia Andreou‡

Departments of Physics and Chemistry, University of Cyprus, P.O. Box 20537, CY1678 Nicosia, Cyprus

Received: May 18, 2005; In Final Form: July 16, 2005

Recent theoretical and experimental studies have shown that polarizable anions, such as iodide and bromide, preferentially accumulate close to the surface of electrolyte solutions. This finding is in sharp contrast to the previously prevailing idea that salts are dielectrically excluded from the free water surface and opens up new avenues for research in specific salt effects. In this work, we have verified the ability of a recently introduced polarizable water model, SWM4-DP, to reproduce this behavior, by simulations of a NaI/water slab, corresponding to a 1.2 M solution. The water and ion polarizabilities are modeled by classical Drude oscillator particles. As revealed by the simulations, a double layer is formed close to the free water surface, with the iodide ions located closer to the interface and the sodium ions at a neighboring, interior layer. Near the surface, all solution species acquire an induced dipole moment, that is perpendicular to the surface and points toward the exterior. The double charge layer causes ordering of water at a subsurface region. Simulations with a simpler system of a single iodide ion in a water slab show that the surface position is stabilized by induced charge interactions; in contrast, the charge−dipole interactions between the iodide permanent charge and the water permanent dipole moment favor the bulk position. Thus, the polarizabilities of ion and water are essential for explaining the increased preference of iodide for the air−water interface, in accordance with other studies.

1. Introduction

Specific salt effects play a very important role in a wide range of physicochemical and biological phenomena, as exemplified by the well-known protein solubility studies of Hofmeister, from more than a century ago.[1] Several studies established that ions can be ordered with increasing salting-in potency from left to right, as follows: SO_4^{2-}, HPO_4^{2-}, OH^-, F^-, $HCOO^-$, CH_3COO^-, Cl^-, Br^-, NO_3^-, I^-, SCN^-, and ClO_4^-. Ions to the left of Cl^- are generally called salting-out ions, water-structure makers, or cosmotropic ions; these ions reduce the solubility of proteins and induce their crystallization.[2] The opposite holds for ions to the right of Cl^-, known as salting-in ions, water-structure breakers, or chaotropic ions. The exact mechanism of action of the Hofmeister ions is not understood to date, but two prevailing schools of thought exist. According to the first explanation,[1−3] specific salt effects occur because ions perturb the water structure, especially close to surfaces or dissolved molecules. Another explanation is based on specific chemical interactions of the ions with groups on surfaces.[3] In recent years, there has been a tremendous renewal of interest in specific salt effects, following the interesting suggestion by Ninham and co-workers that they stem from dispersive interactions between the ions and any dielectric interface, including dissolved biomolecules.[4,5] This implies that the hitherto overlooked role of ionic polarizability must be re-examined.

Probably the best model system for a fundamental understanding of specific salt effects is the free water surface of electrolyte solutions, since it does not contain any chemical groups that can specifically interact with the ions. The surface tension of electrolyte solutions has been measured for a large number of electrolytes over large concentration ranges. From these measurements, it was established that surface tension increases linearly with electrolyte concentration[6] and depends strongly on the anion and less strongly on the cation of the electrolyte. The increase of surface tension was taken as a proof that ions are dielectrically excluded from the free water surface,[7] since they must pay a very high energetic penalty upon losing some of their hydration shell. This picture of the electrolyte solution−air interface was sharply challenged in recent years by computer simulations of ions in water clusters[8−18] or at the planar water−air interface.[19−25] The early experimental and theoretical work focused on small ion−water clusters. Perera and Berkowitz first showed by simulations with a polarizable water and ion force field[8,9,15] and analysis of photodetachment spectra[10,26] that large halide ions (Cl^-, Br^-, and I^-) were attached to the surface of small water clusters. Dang and co-workers with classical simulations[11,12] and Xantheas[13] with quantum calculations also proved the asymmetrical solvation of halide ions in small water clusters. Stuart and Berne[14,16] showed that the surface solvation of chloride persisted even for very large clusters (up to 255 water molecules). They argued that ionic or even water polarizability was not important, provided the water model had a large dipole moment. Recent, very long simulations by Herce et al.[18] with a 238-water-molecule cluster have shown that the main cause of surface solvation is the induced polarization on water and ion, coupled to the ion charge and size.

Stuart and Berne argued in a 1999 paper[16] that interfacial solvation is enhanced by the cluster curvature and does not occur at planar interfaces. This conclusion was supported by earlier

* To whom correspondence should be addressed. E-mail: archonti@ucy.ac.cy (G.A.); psleon@ucy.ac.cy (E.L.).
† Department of Physics.
‡ Department of Chemistry.

10.1021/jp0526041 CCC: $30.25
Published on Web 09/07/2005

simulations with a nonpolarizable water model.[27] However, more recent computer simulations[19−25] have shown that large polarizable ions are indeed preferentially solvated close to the water surface even for the planar interfaces of electrolyte solutions. Tobias and co-workers showed that ionic surface solvation is weakly related to the actual size of the ion but is strongly connected to the polarizabilities of both the ions and the water molecules.[21−23] They also showed that an increase of the surface tension can be consistent with the enhanced presence of solute at the interface, as long as there is an adjacent depletion region of sufficient size, yielding a negative Gibbs surface excess of the solute.[22]

These simulation results are supported by several spectroscopic methods to various extents, depending on the method used. Weber et al.[28] studied aqueous alkali halide solutions by photoelectric emission experiments; they concluded that the region near the surface is depleted of ions but could not rule out an enhancement of ion concentration at the surface, because the probing depth of their experimental method was larger than the width of a single molecular layer. Raymond and Richmond[29] studied the surfaces of aqueous NaF, NaCl, NaBr, and NaI solutions with vibrational sum-frequency spectroscopy (VSFS); they argued that the hydrogen bonding of the water in the topmost surface layer is not altered significantly, implying a diminished anion population at the surface region. However, Allen and co-workers[30] concluded on the basis of VSFS, Raman, and IR studies that the hydrogen-bonding network of water molecules in the interfacial region of NaBr and NaI solutions is perturbed and the interfacial depth of the solution is increased. Tobias and co-workers computed the VSFS spectra of a NaI solution;[23] they attribute the differences between the solution and neat water spectra to enhanced ordering of water in a subsurface region, which may be caused by the formation of a double ion layer at the surface. In our simulations, we also observe this subsurface water ordering (see below). Saykally and co-workers[31,32] estimated a negative surface excess free energy of iodide and azide at the water−air interface by second-harmonic generation experiments. Hemminger and co-workers[33] used X-ray photoelectron spectroscopy to study the liquid−vapor interface of potassium bromide and potassium iodide; their experiments measure an anion enhancement at the interface, that is stronger than the simulation predictions.[19,21]

The accumulated evidence from simulations and experiments supports the presence of ions at the air−water interface. However, the interpretation of experimental spectra is difficult,[23,29,30] and quantitative discrepancies between simulations and experiments remain;[33,34] thus, detailed comparisons between experimental studies and simulations of ions at interfaces are needed.[34] Simulations of these systems with different water and ion models are particularly useful, because they provide independent theoretical evidence for or against the surface solvation picture. Furthermore, the comparison with the existing theoretical and experimental results aids in confirming the accuracy of the new models.[33,34]

In the present work, we conduct simulations of the air−water interface of a sodium iodide solution, using a very recently developed polarizable model for water[35] and ions,[36] which models polarizabilities using classical Drude oscillators attached to the oxygen atoms of water and ions.[37] The model has proved to be very successful in reproducing a wide range of liquid-phase water properties, including the dielectric constant and the surface tension.[35] Besides being computationally efficient, it allows a transparent partitioning of the total interaction energy into components due to permanent and induced charge distributions. Furthermore, it allows a straightforward examination of the components of the induced dipole moment on the ions and the water molecules close to the surface. We have focused on a NaI solution in our simulations, since Jungwirth and Tobias[21−23] have provided several key results for this system. Furthermore, iodide is an important chaotropic ion, which always exhibits specific effects much stronger than those of the more investigated chloride.

In our simulations, the iodide ions are indeed preferentially located at the interface and the sodium ions at an adjacent, interior layer, in agreement with refs 21−23. The ions and water molecules acquire induced dipole moments, the directions of which are perpendicular to the interface, while their magnitudes depend on the polarizability of the various species. The induced average dipole moments of all three species (iodide, sodium, and water) point toward the free water surface. In a region 3−5 Å below the surface, we observe an orientation of the water permanent dipole moments toward the interface, in agreement with ref 23.

To understand further the observed attraction of iodide for the water surface, we conduct additional calculations with a simpler system, consisting of a single iodide ion in a water slab. In separate simulations, the iodide is restrained at the center of the water slab, or at a position near the free water surface. At the ion−water interface, a positive polarization charge is developed, due to the orientation of the water permanent and induced dipole moments in response to the ion field. The polarization charge is asymmetrically distributed around the iodide at the free water surface, inducing a larger dipole moment on the ion. The surface position is stabilized by dipolar interactions, in which the induced dipole moments on iodide and water play a major role; in contrast, the charge−dipole interactions between the iodide permanent charge and the water permanent dipole moment favor the bulk position. Thus, polarizability is essential for the increased preference of iodide for the free water surface in agreement with other works.[18,20−23]

The next section describes the model and simulation methods. We then present the results for the NaI solution and single-iodide-ion simulations. The last section presents the conclusions of this work.

2. Model and Simulation Methods

Water and Solute Model. The water and ion parameters are listed in Table 1. The water is described by the polarizable "SWM4-DP" model, which was developed recently.[35,37] As shown in ref 35, the model well reproduces various water properties, particularly the water bulk dielectric constant (79) and the surface tension (66.9 dyn/cm).[35] More recently, the same model has been combined with a new, polarizable model for ethanol and has been tested in simulations of water−ethanol mixtures at various concentrations; the simulations reproduce the energetic and dynamical properties of the mixtures as well as the mixture dielectric constant.[38] A first step toward a systematic development of a polarizable force field based on the Drude oscillator has also been described in ref 39.

The sodium and iodide ions correspond to charged van der Waals spheres; ionic polarizability is taken into account by attaching Drude particles on the ions (see Table 1). The ion parameters were supplied to us by G. Lamoureux, ahead of publication. Their parametrization is described in detail in ref 36.

NaI Simulations. The NaI simulation system consisted of 1000 water molecules, 22 sodium particles, and 22 iodide particles. To model the free water surface, we followed a well

TABLE 1: Parameters Used for the Simulation System[a]

water geometry: $l_{OH} = 0.9572$ Å; $l_{OOM} = 0.238\,08$ Å; ∠HOH = 104.52°; ∠HOOM = 52.26°				
	charge (e^-)	ϵ (kcal/mol)	σ (Å)	α^b (Å^3)
water				1.042 52[c]
O	−1.771 85[b]	0.205 68	3.180 30	
DO	1.771 85[b]			
OM	−1.107 40			
H1/H2	0.553 70			
sodium[d]				0.157[e]
Na	0.6876[f]	0.031 51	2.583 606	
DNa	0.3124[b]			
iodide[d]				7.439[g]
I	−5.7331[f]	0.1591	4.917 76	
DI	4.7331[b]			

[a] The water molecule (SWM4-DP) is a four-site model, with an additional classical Drude oscillator particle attached to site O. The model and its parametrization are described in ref 35. The geometry of the water molecule is fixed at the gas-phase experimental values.[51] Throughout the table, D*X* denotes a Drude particle of $m = 0.4$ au, attached to atom *X*. [b] The induced charge, q_{DX}, is linked to the polarizabilities, α, via the relation $\alpha = q_{DX}^2/k_{DX}$, with k_{DX} being the force constant of the harmonic spring between Drude particle D*X* and its heavy partner, *X*.[35] For all species, the force constants were set to $k_D = 1000$ kcal/mol/Å^2.[35,36] [c] From ref 35. [d] Parameters supplied by Lamoureux, ahead of publication.[36] [e] From Mahan.[36,52] [f] For sites I and Na, the total (permanent + induced) charge is listed. [g] From time-dependent ab initio calculations at the MP2 level, that include relativistic effects,[36,53] a scaling factor of 0.724 was applied, as explained in ref 36.

established procedure,[20−22,40,41] according to which a cubic solution is simulated under periodic boundary conditions, with the unit cell elongated in one direction. With this arrangement, two interfaces are created perpendicular to the elongated direction and the solution system corresponds to a slab.

Our interface simulations employed a constant volume tetragonal unit cell with the dimensions 31.49 × 31.49 × 95.0 Å^3. In the initial setup of the simulations, we performed runs under a constant pressure of $P = 1$ atm and a constant temperature of $T = 300$ K and under cubic periodic boundary conditions. The average size of the fluctuating unit cell (31.49 Å) in the constant *T*, *P* simulations was used to set the fixed length of the tetragonal unit cell *x* and *y* dimensions in the interface simulations.

All simulations were conducted with the molecular mechanics program CHARMM.[42] The electrostatic interactions were calculated without truncation by the particle-mesh Ewald method,[43] with the parameter $\kappa = 0.333\,33$ for the charge screening and sixth-order splines for the mesh interpolations. The Lennard-Jones interactions between atom pairs were shifted to zero at a cutoff distance of 15 Å. The Drude oscillation amplitudes were controlled by a low-temperature (1 K) Nose−Hoover thermostat, acting on the local center-of-mass reference frame of each D−*X* pair;[37] the relaxation time of the thermostat was set to 0.005 ps. It was shown previously that the resulting Drude-particle trajectories are in good agreement with the self-consistent field regime.[37] A second Nose−Hoover thermostat (at room temperature) was applied to the center of mass of the D−*X* pairs and the water hydrogens; for this thermostat, the relaxation time was set to 0.1 ps. The water molecules were retained to the experimental geometry by the SHAKE/Roll and RATTLE/Roll procedures,[44] implemented into CHARMM.[37] A multistep integration procedure was used for the thermostat variables, with $n_c = 100$. With this scheme, stable trajectories with a 1 fs time step were obtained. In the initial, cubic-cell runs, the pressure was maintained constant by coupling the system to a modified Andersen−Hoover barostat,[45] implemented into the CHARMM program.[37] The barostat relaxation time was 0.1 ps.

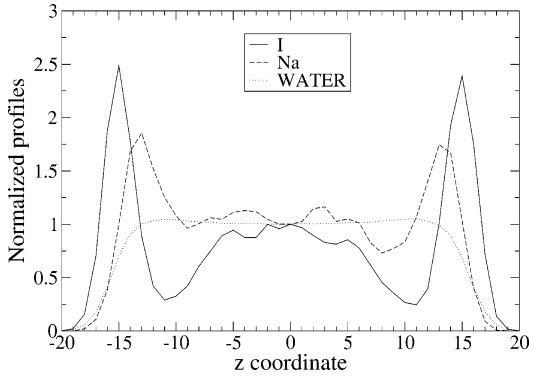

Figure 1. Profile of iodide, sodium, and water as a function of the *z* coordinate, in simulations of a water slab with 1000 water molecules, 22 sodium cations, and 22 iodide anions, modeling the free water surface of a 1.2 M NaI/water solution. The value $z = 0$ corresponds to the center of the water slab employed in the simulations. The profiles have been normalized with respect to the value at $z = 0$. The free water surfaces are perpendicular to the *z*-direction.

Single-Iodide-Ion Simulations. In these simulations, the systems consisted of 1000 water molecules and a single-iodide-ion solute. To create a water slab, a tetragonal unit cell was employed in the interface simulations, with a constant volume and the dimensions 31.05 × 31.05 × 93.3 Å^3. The slightly reduced size (31.05 Å, compared to 31.49 Å in the NaI simulations) was determined from several hundred picosecond runs of the same system under cubic boundary conditions in $T = 298$ K and $P = 1$ atm; a 31.05 Å cubic cell containing 1000 water molecules is consistent with the experimental water number density, 0.0334 molecules/Å^3. The iodide was restrained at the center of the water slab or at a point near the surface ($z = 14.5$ Å), by a harmonic constant of 7 kcal/mol/Å^2. The other conditions were the same as those in the NaI simulations.

3. Results

3.1. NaI Solution. To collect statistics, 12 independent constant *T*, *V* molecular dynamics simulations of the solution slab were conducted. The starting coordinates were taken from various snapshots along 500 ps long trajectories of a bulk-water NaI solution, generated under constant $T = 300$ K and $P = 1$ atm conditions. Each of the 12 solution-slab simulations had a duration of 600 ps. The density profiles were calculated by extracting coordinates from the last 300 ps of each simulation; thus, the resulting profiles correspond to a run with a total length of 3.6 ns.

The sodium, iodide, and water oxygen density profiles are shown in Figure 1 as a function of the *z* coordinate (the direction, vertical to the free water surface). Each profile is normalized with respect to its value at the center of the slab ($z = 0$). Examination of the profiles shows that the two ionic species form a double layer at the interfaces. The iodide profile has a prominent peak of 2.5 at $z = \pm 15$ Å, followed by a region (± (7−12) Å) where the iodide ions are depleted. The increased iodide concentration at the surface drives the accumulation of sodium ions at a nearby layer; this is indicated by a peak in the sodium profile with a height of 1.9 at $z = \pm 12.5$ Å, adjacent to the iodide peak but shifted toward the interior of the slab. The resulting profiles are very similar to the ones obtained by Jungwirth and Tobias[21,22] in a study of a 1.2 M NaI/water solution (modeled by 864 water molecules, 18 sodium ions, and

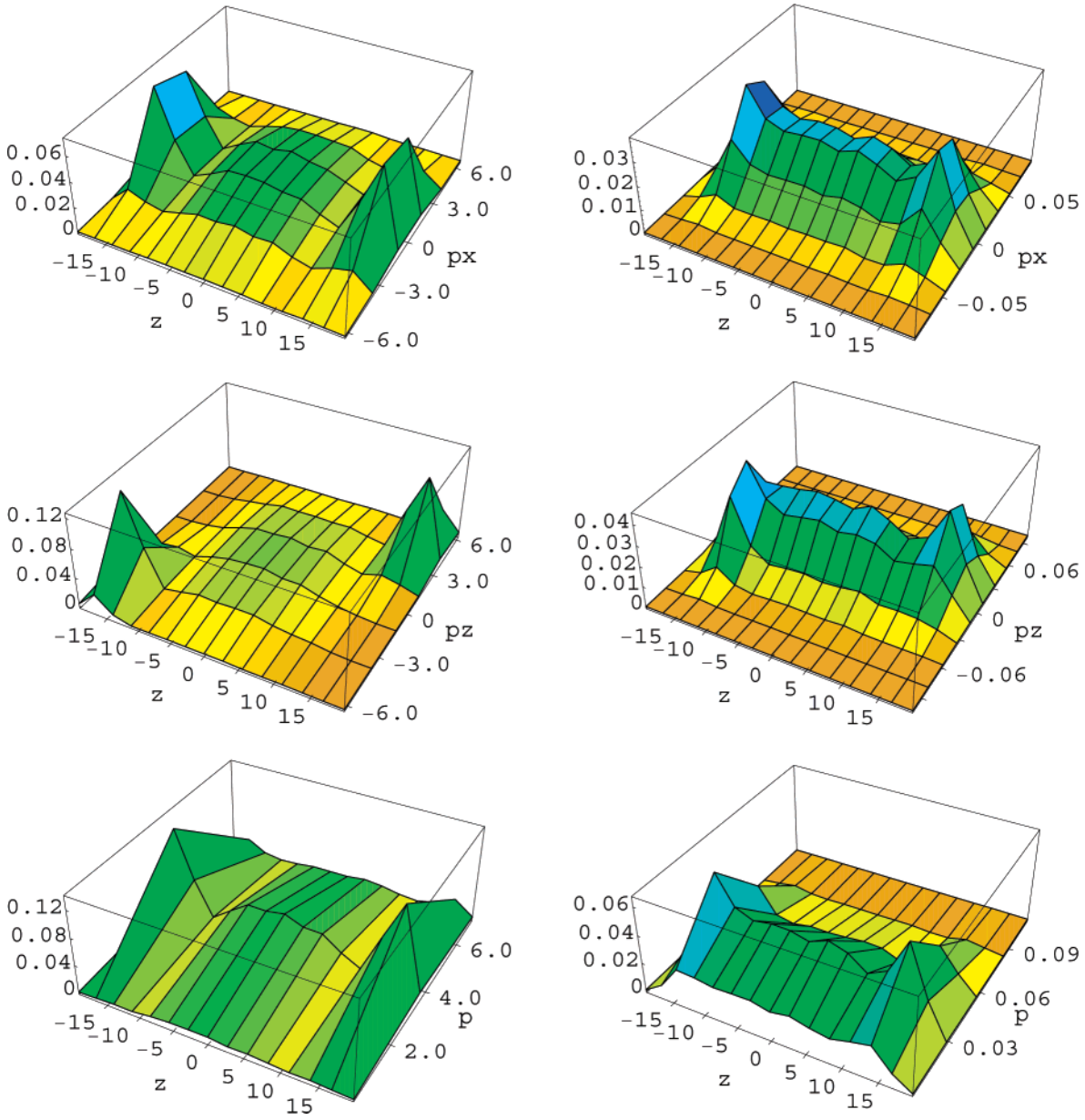

Figure 2. Two-dimensional probabilities, $P(z, p_i)$, to observe an iodide ion (left panel) or sodium ion (right panel) with *induced* dipole moment p_i at position z, obtained from the NaI solution simulations. The free water surfaces are perpendicular to the z-direction, and the center of the water slab corresponds to the position $z = 0$. In each panel, the probabilities for the p_x and p_z components and magnitude p of the induced dipole moment are shown, respectively, in the upper, middle, and lower plots. The probabilities of the p_x and p_y components are very similar; therefore, the latter is omitted.

18 iodide ions), even though their polarizable water and ion models are entirely different from the ones employed here.

To analyze the change in the polarization of the solute and water near the surface and the bulk, we calculated the induced ion and the induced and permanent water dipole moments, as a function of the distance from the free water interface. The two-dimensional probabilities for the various dipole moment components are shown in Figures 2 and 3. For all species, the probabilities of the p_x and p_y components are very similar; we include only the former. All dipole moments are expressed in units of debyes (D).

The iodide components are shown on the left panel of Figure 2. The probability of the p_x component has two distinct, symmetric peaks, centered around $z = \pm 15$ Å and $p_x = 0$; the same holds for p_y. This is expected, due to the symmetry of the water slab along the directions x and y. For the p_z component, the two probability peaks are shifted in opposite directions along the p_z axis. On the positive-z interface ($z = 15$ Å), the peak is located at a value of $p_z \approx +4.0$ D. Since the charge on the iodide Drude particle is positive by convention (see Table 1), the observed dipole moment sign indicates that, on this interface, the Drude iodide particle is positioned to the exterior of its heavy-atom partner; the same holds at the negative-z ($z = -15$ Å) interface. Thus, at both interfaces, the induced dipole moment points away from the bulk, and the polarizable iodide particles present an increased, effective negative charge toward the bulk. The corresponding probability for the total magnitude of the induced dipole moment is shown at the bottom of the left panel of Figure 2. The iodide particles have an increased induced dipole moment at the interface, due to the p_z component. The average dipole moment of iodide in the entire solution slab is 3.77 D, a very considerable value.

The corresponding probabilities for sodium are shown in the right panel of Figure 2. As in the iodide case, the p_x and p_y

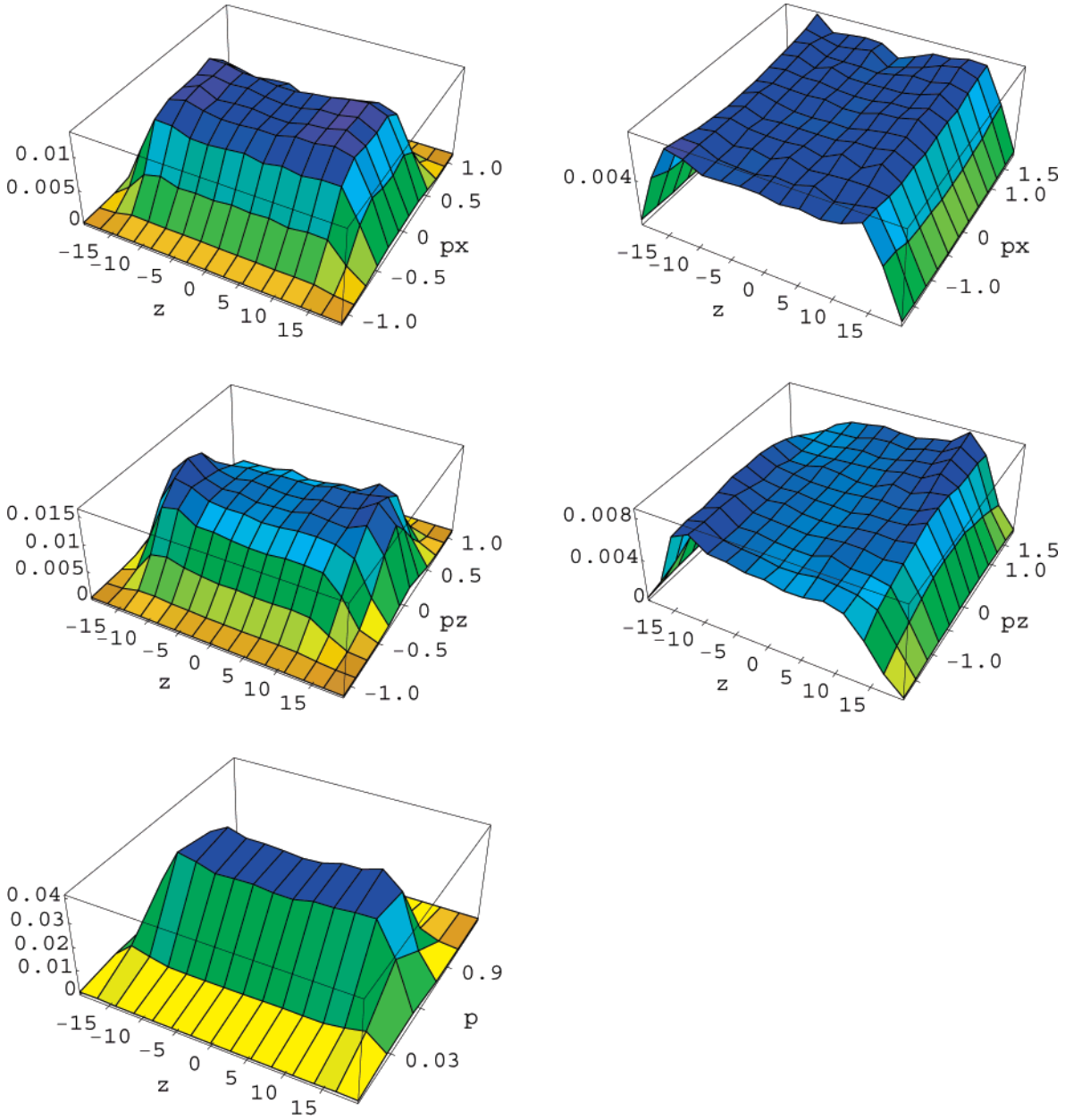

Figure 3. Two-dimensional probabilities for the water dipole moment components, obtained from the NaI solution simulations. (left panel) The probabilities for the *induced* p_x and p_z components and total magnitude p are shown, respectively, in the upper, middle, and lower plots. (right panel) The corresponding plots for the *permanent* p_x and p_z components are shown in the upper and lower plots.

components have symmetric peaks, centered at $z = \pm 12.5$ Å and $p_x = p_y = 0$. In the case of the p_z component, the probability peaks are centered at $(z, p_z) \approx \pm(12.5$ Å, 0.03 D); the observed p_z-component signs indicate that the induced dipole moment on sodium ions near the interfaces points toward the exterior of the slab. Thus, the polarizable sodium particles present an increased, effective positive charge toward the iodide particles. The two-dimensional probability for the magnitude of the induced dipole moment is included at the bottom of the right panel in Figure 2. The sodium particles have an increased induced dipole moment at the interface, due to the p_z component. The average dipole moment of sodium throughout the solution slab is 0.03 D. Thus, the induced dipole moment is significantly smaller on sodium with respect to iodide, in accordance with the smaller polarizability of the former.

For water, the two-dimensional probabilities of the *induced* dipole moment are shown on the left panel of Figure 3. In the case of the p_x and p_y components, the probabilities are flat, reflecting the symmetry of the water slab along these two directions. The p_z component has two weak and somewhat broad peaks, slightly shifted toward, respectively, positive and negative p_z values in the region $\pm(12-14)$ Å, that is, at the region of the charge layer. As in the previous cases, the two signs correspond to configurations in which the water molecules near the interfaces orient their Drude particles away from the bulk. The probability for the total magnitude, p, of the induced dipole moment is shown in the lower left panel. In the region $\pm(6-16)$ Å, the probability is flat and centered around 0.6 ± 0.1 D. At the interface ($|z| \geq 15$ Å), the region of nonzero probability is somewhat wider, extending to values of small p. This indicates that the induced dipole moment on water has the tendency to decrease away from the bulk (see also below and Figure 4). In summary, the water acquires a stable (nonzero) z component of induced dipole moment at the two interfaces, but its total (induced) dipole moment increases toward the bulk

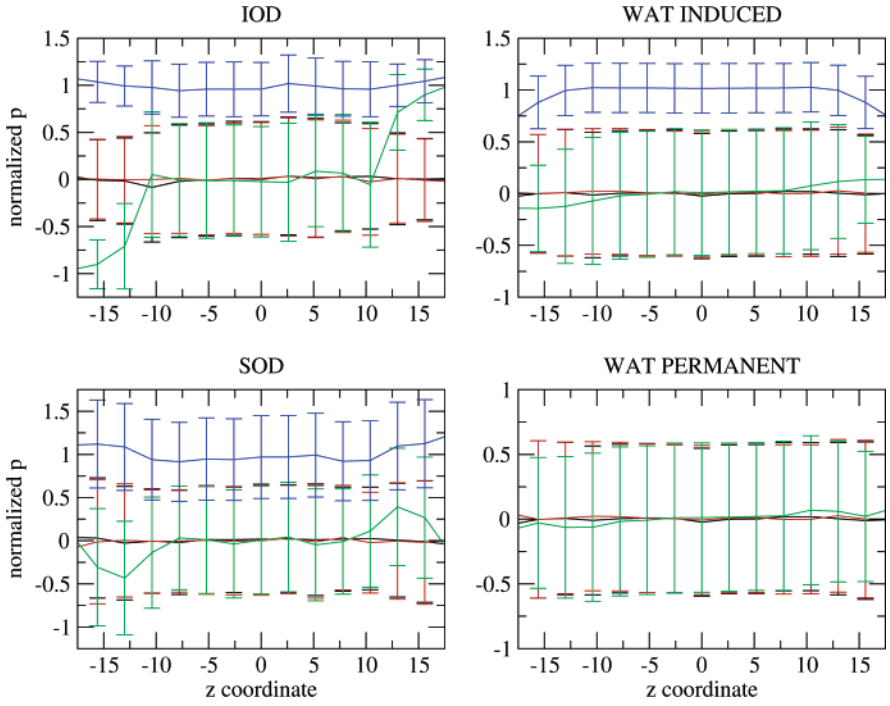

Figure 4. Variation of the average dipole moment components and total magnitude, as a function of the position z along the direction vertical to the interface, obtained in the NaI simulations. Each component has been divided by the average dipole moment, $\langle p \rangle$, of the same species in the entire slab (3.77 D (I), 0.03 D (Na), 0.63 D (induced water components), 1.85 D (permanent water components), respectively). Black, component $\langle p_x(z) \rangle$; red, component $\langle p_y(z) \rangle$; green, component $\langle p_z(z) \rangle$; blue, magnitude $\langle p(z) \rangle$. The p_x and p_y curves practically coincide, as expected due to the symmetry of the solution slab along these two directions. The normalized standard deviations of the dipole moments are shown as error bars.

phase. The average induced dipole moment of water in the entire solution slab is 0.63 D.

The two-dimensional probabilities for the water *permanent* dipole moment are shown on the right panel of Figure 3. The probabilities of the two components p_x and p_y are uniform throughout the slab. Thus, in these directions, the water molecules are randomly oriented, as expected. In the case of the p_z component, the probability is uniform in the interior of the slab but acquires weak peaks at $z \approx \pm 12$ Å and $p_z \approx \pm 1.7$ D, that is, close to the extremum values (± 1.85 D). Thus, in this region, which is $\approx$3.0 Å below the surface and near the iodide/sodium double layer, a small number of water molecules are oriented toward the double layer. This is in agreement with the results of a recent study of an aqueous iodide interface by Tobias and co-workers,[23] where water molecules were found to be ordered at approximately one water layer below the Gibbs dividing surface (see also below).

Using the two-dimensional probabilities described above, we calculated the average dipole moment components, $\langle p_i^X(z) \rangle$, for each species X, as a function of the z coordinate; for example, $\langle p_z^{SOD}(z_0) \rangle$ is the average z component of the dipole moment for sodium ions located on the plane $z = z_0$. The components are shown in Figure 4; normalized values are obtained by dividing each component, $\langle p_i^X(z) \rangle$, of a particular species X by the average magnitude of the dipole moment for the same species, $\langle p^X \rangle$, obtained in the entire solution (0.03 D (Na), 3.77 D (I), and 0.63 D (water), respectively). The water permanent components are divided by 1.85 D, the magnitude of the permanent dipole moment of water. The normalized root-mean-square (rms) deviations of the dipole moment components are also included in the same figure as error bars.

The average components of the iodide induced dipole moment are near zero for values of $|z| < 10$ Å. In the same region, the corresponding (normalized) standard deviations are $\approx 0.63 \approx {}^1/_2({}^\pi/_2)^{1/2}$; this is the expected ratio, $(\langle x_i^2 \rangle)^{1/2}/\langle r \rangle$, for a three-dimensional vector with magnitude r and components x_i following a Gaussian distribution with a zero mean. Thus, in this region, the dipole moment components are randomly oriented. For values of $|z| > 10$ Å, the average $\langle p_z \rangle$ departs from zero, in agreement with the probability $P(z, p_z)$ discussed above. For $|z| \geq 12$ Å, the normalized p_z value is larger than the corresponding normalized rms deviation, signifying that the iodide p_z component fluctuates but retains its sign. The average magnitude, $\langle p(z) \rangle$, becomes slightly larger close to the interface, due to the p_z contribution.

Analogous comments hold for the corresponding components of the sodium ion. The average z component departs from zero at $|z| \approx 10$ Å and has extremum values at $z \approx \pm 12.5$ Å, that is, at the position where these ions are localized in the double layer. At these positions, the rms deviation is $(\langle \delta p_z^2 \rangle)^{1/2} > \langle p_z \rangle$; thus, close to $z = 12.5$ (-12.5) Å, the average sodium p_z component is positive (negative), but the values for individual ions can change sign due to thermal fluctuations. The average x and y components are small throughout the slab, as expected. The average magnitude, $\langle p(z) \rangle$, is slightly increased close to the interface.

The induced dipole moment of water is shown in the right upper plot of Figure 4. Its average magnitude has a maximum value at the bulk and decreases uniformly toward the interface. The z component acquires positive (negative) values at $|z| > 8$ Å. This signifies that some of the water molecules close to the interface have an induced dipole moment that is oriented along the z-direction and points away from the bulk, in accordance with the probability plots discussed above.

The permanent water components are included in the lower right plot of Figure 4. The p_x and p_y components behave like random Gaussian variables centered around zero, throughout the slab. Near the sodium and iodide density profile peaks (at $|z| \geq \approx 10$ Å), the normalized value of the z component is $\approx \pm(0.05 \pm 0.5)$ and points toward the interface. Taking into

account the normalization factor (1.85 D), this value corresponds to $p_z \approx \pm(0.09 \pm 0.9)$ D. Thus, in this subsurface region, we observe some ordering of the water structure, that is caused by the double charge layer. Tobias and co-workers have suggested in ref 23 that this ordering is responsible for the increase in intensity of a sodium iodide solution sum-frequency spectrum around 3400 cm^{-1} compared to neat water−air and provides evidence for the formation of the double charge layer at the interface.

The normalized value for the induced component $\langle p_z \rangle$ in the same region is $\pm(0.15 \pm 0.35)$, as seen in the upper right plot. Multiplying by the normalization factor (0.63 D) yields a value of $\approx \pm(0.09 \pm 0.22)$ D. Thus, the induced and permanent average water components $\langle p_z \rangle$ are comparable at the interface, but the former fluctuates to a much smaller extent; that is, it interacts more strongly with the field of the double layer.

From the above results, it follows that the thermodynamically dominant structure of the solution corresponds to the development of an inhomogeneous distribution of the solute permanent charge at the free water surface, with the negative charge (iodide ions) at the exterior and the positive charge (sodium ions) at the interior of the solution. This arrangement of permanent charges induces a dipole moment on the solute and solvent particles, with a direction that is perpendicular to the interface and a magnitude that depends on the polarizability of the various species. In all three species (iodide, sodium, and water), the induced average dipole moments point away from the bulk close to the interface; this alignment is presumably stabilized by the ionic charge distribution and by the water permanent dipole orientations in the vicinity of the ions (see also below).

3.2. Simulations of a Single Iodide Particle in a Water Slab. To obtain a better understanding of the reasons that stabilize the previously described solute arrangement, we studied a simpler system, consisting of 1000 water molecules and a single iodide particle. We focused on the iodide ion, as it demonstrates here and in other studies[21,22] the most pronounced preference for the interface. Nevertheless, these results illuminate also the lack of sodium attraction for the interface. We carried out two simulations. In one simulation, the solute was harmonically restrained at the center of the water phase; in the other, the solute was restrained at $z = 14.5$ Å, on the positive-z interface. Both simulations had a total duration of 700 ps. The analysis employed the last 500 ps portion of the trajectories.

The solute−oxygen and solute−hydrogen radial distribution functions are shown in Figure 5. For both pairs, the contact peaks are markedly pronounced, when the solute is restrained at the water surface. Thus, in accordance with its preference for the interface in the NaI solution simulations, the isolated iodide forms stronger local interactions with water molecules at the interface. The total iodide−water interaction energy depends also on the number of surrounding neighbors in each case. A plot of the corresponding coordination numbers as a function of the distance from iodide is shown in the lower panel of Figure 5. At the edge of the solute−oxygen contact peak ($r \approx 4.0$ Å), the number of surrounding oxygens is ≈6.7 and ≈5.3, respectively, when iodide is at the center of the bulk and at the surface position. At an iodide−oxygen distance of $r = 5$ Å, the corresponding numbers are ≈16 and ≈9.5; that is, the iodide is surrounded by roughly twice as many waters in the bulk.

To compare the iodide−water interactions at the surface and in the bulk, we calculated the corresponding average interaction energies at the two positions; the results are listed in Table 2. To assess the relative importance of the permanent and induced

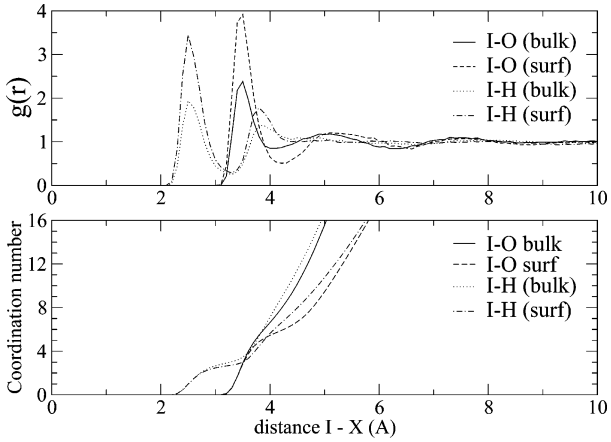

Figure 5. Iodide−water radial distribution functions, evaluated by simulations of a single iodide molecule in a water slab. The iodide was restrained at the center of the slab (bulk) or at the plane $z = 14.5$ Å, on the free water surface (surf). (upper panel) Radial distribution functions. (lower panel) Corresponding coordination numbers. In these plots, "O" refers to the O atom of the water model (see Table 1).

TABLE 2: Decomposition of the Iodide−Water Energy into Contributions from Induced and Permanent Charges, in the Single-Iodide-Ion−Water Simulations[a]

component	bulk[b]	surf[b]	difference
I_p-W_p[c]	−114.3	−107.3	+7.0
I_p-W_i	−27.3	−28.6	−1.3
I_i-W_p	−16.9	−19.3	−2.4
I_i-W_i	−3.3	−4.2	−0.9
total	−161.7	−159.3	+2.4
Contribution from First Hydration Shell			
I_p-W_p[c]	−38.4	−35.7	+2.7
I_p-W_i	−6.13	−6.27	−0.14
I_i-W_p	−13.0	−15.0	−2.0
I_i-W_i	−2.24	−2.92	−0.68
total	−59.8	−59.9	−0.1

[a] All energies are in kilocalories per mole. [b] Iodide is respectively restrained in the center (bulk) or the interface (surf) of a water slab. [c] "I" and "W" respectively denote iodide and water; "p" and "i" denote permanent and induced charge (see also text). The average number of water molecules in the first hydration shell is 5.3 (surface) and 6.7 (bulk), respectively.

charges, we decompose the total iodide−water energy into contributions from the permanent (p) and induced (i) charges.

As shown in this table, the interaction between the permanent charges on the iodide and the permanent charges (permanent dipole moment) on water (entry "I_p-W_p") favors the location of iodide in the center of the water slab. However, the three other components stabilize the interfacial position. All of these components involve the induced charges on the ion, water, or both. This indicates the importance of polarizability in stabilizing the interfacial location of iodide. Among the three last components, the most important relative difference (−2.4 kcal/mol) is due to the term I_i-W_p, that is, the dipole−dipole interaction between the induced dipole moment of iodide and the permanent dipole moment on water.

To assess the importance of local versus distant ion−water interactions, we include in the same table the various interaction terms between iodide and water molecules in the first hydration shell. Despite the smaller average number of waters surrounding iodide at the surface position (5.3), compared to the bulk position (6.7), the total interaction energies are approximately equal (−59.8 kcal/mol in the bulk compared with −59.9 kcal/mol at the surface). Thus, iodide interacts more strongly with water molecules at the surface position, in accordance with the more

TABLE 3: Relative Orientation and Magnitude of Iodide and Nearest-Neighbor Water Dipole Moments in the Single-Iodide-Ion Simulations

property	surface	bulk
$\langle\theta_{\vec{I}_i}\rangle^a$	24.9(13.1)	91.7(36.3)
$\langle\theta_{\vec{OI}-\vec{W}_p}\rangle$	51.0(4.6)	56.5 (6.7)
$\langle\theta_{\vec{OI}-\vec{W}_i}\rangle$	43.6(6.4)	53.3 (7.3)
$\langle\theta_{\vec{W}_p-\vec{W}_i}\rangle$	21.1(4.7)	19.4(4.1)
$\langle\theta_{\vec{OI}-\vec{I}_i}\rangle$	58.3(6.0)	73.6(9.5)
$\langle\theta_{\vec{I}_i-\vec{W}_i}\rangle$	67.2(11.6)	79.9(13.5)
Single-Iodide-Ion Simulations		
$\langle p_z^{IOD}\rangle^b$	3.03(0.6)	−0.08(1.7)
$\langle p^{IOD}\rangle^b$	3.42(0.5)	3.07(0.8)
$\langle p^{WAT}\rangle^b$	0.67(0.06)	0.66(0.06)
NaI Simulations		
$\langle p_z^{IOD}\rangle^c$	3.40(1.0)	−0.07(2.2)
$\langle p^{IOD}\rangle^c$	3.92(0.8)	3.62(1.1)
$\langle p^{WAT}\rangle^{c,d}$	0.57(0.16)	0.64(0.15)

[a] The various angles are explained in Figure 6. $\vec{OI}$ is the water oxygen−iodide vector; $\vec{I}_i$ is the iodide induced dipole moment vector; $\vec{W}_p$ and $\vec{W}_i$ are the water permanent and induced dipole moment vectors. [b] Average induced dipole moments (in debyes) in the single-iodide-ion−water simulations. [c] Average induced dipole moments (in debyes) in the NaI simulations. They correspond to the normalized values of Figure 4, multiplied by the appropriate normalization factor (see caption of Figure 4 and corresponding text). [d] These values are not averaged over the water molecules in the first hydration shell of ions but over the total number of water molecules at the $z = 0$ plane (bulk position) or the $z = 15.0$ plane (surface position).

pronounced radial distribution functions (Figure 5). The interactions between the induced charges on iodide and the permanent or induced charges on water contribute, respectively, −2.0 and −0.68 kcal/mol to the stabilization of the surface position; these values are equal to 83 and 76% of the corresponding values in the entire slab; thus, the dipole−dipole interactions between iodide and water are most significant near the ion, as expected. In contrast, the charge−dipole interactions (between the iodide permanent charge and the water permanent or induced dipole moment) extend beyond the nearest waters. It is noteworthy that the contribution from the term I_p-W_i is −0.14 kcal/mol in the first hydration shell, but the total value of the same term is significantly larger (−1.3 kcal/mol). The induced dipole moment on water molecules in the iodide hydration shell is the same in the bulk and surface positions (see below and Table 3), explaining the small value (−0.14 kcal/mol). Nevertheless, the water polarizability is still important for the iodide attraction at the surface, due to interactions that extend beyond the first hydration shell of the ion.

The average orientation of water molecules in the first hydration shell of iodide can be characterized in terms of the angles between the water oxygen−iodide vector, $\vec{OI}$, the vectors of the water permanent, $\vec{W}_p$, and induced, $\vec{W}_i$, dipole moment, and the iodide dipole moment, $\vec{I}_i$. These angles and vectors are shown schematically in Figure 6; the corresponding average values and standard deviations from the simulations are included in Table 3.

The average angle between the iodide induced dipole moment and the *Oz* axis, $\langle\theta_{I_i}\rangle$, is 24.9° at the surface and 91.7° in the bulk position. Thus, at the surface, the iodide induced dipole moment points away from the bulk, as in the NaI solution simulations. The angle between the water permanent dipole moment, $\vec{W}_p$, and the oxygen−iodide vector ($\vec{OI}$), ($\theta_{\vec{OI}-\vec{W}_p}$), is 51.0° at the surface, that is, approximately equal to half of the water molecular angle ∠HOH (104.52°). This signifies that the water molecules at the surface hydration shell orient one

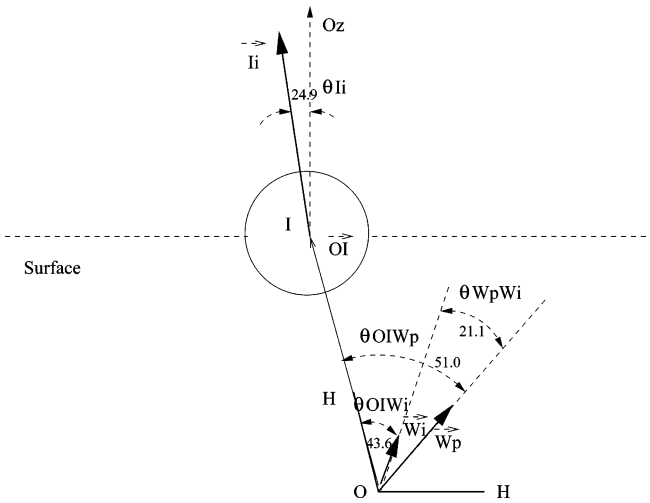

Figure 6. Definition of angles used to describe the average orientation of water molecules in the hydration shell of iodide, in the single-iodide-ion−water simulations (see also text and Table 3). $\vec{OI}$ is the water oxygen−iodide vector; $\vec{I}_i$ is the iodide induced dipole moment vector; $\vec{W}_p$ and $\vec{W}_i$ are the water permanent and induced dipole moment vectors. The average angles for the hydration shell, when iodide is restrained at the surface position, are shown in the figure. The angles and magnitude of dipole moment vectors are not drawn to scale.

hydrogen directly toward the iodide, forming a linear hydrogen bond. In the bulk, the same angle is slightly larger (56.5°); thus, the linear arrangement of the water oxygen−hydrogen−iodide is less satisfied. The water induced dipole moment, $\vec{W}_i$, is oriented somewhat closer to the iodide; the corresponding angle, ($\theta_{\vec{OI}-\vec{W}_i}$), is ≈43.6 and ≈53.3° in the surface and the bulk. The water permanent and induced dipole moments are not collinear, but the average angle between them is relatively small (21.1 and 19.4°, respectively).

The geometry of the iodide hydration shell and the average strength of the various interactions described above (Table 2) imply a mechanism of iodide attraction at the surface in agreement with what has been suggested by other workers.[20,21] According to this mechanism, the field of the iodide permanent charge and the water polarity force the water molecules near the iodide to adopt orientations in which they form one linear hydrogen bond with the ion. Furthermore, the iodide field induces a dipole moment on the proximal water molecules, that points toward the iodide. The orientation of the permanent and induced water dipole moments corresponds to an excess of positive polarization charge around the iodide. When the iodide is close to the water surface, this polarization charge lacks spherical symmetry, inducing a larger average dipole moment on iodide (see below and Table 3). The iodide−water dipole moment interactions are also stronger at the surface (Table 3), contributing to the preference of iodide for this position.

In the single-iodide-ion simulations, the total electrostatic interaction energy favors weakly the bulk position. Assuming that the electrostatic free energy is well described by a linear-response approximation[46,47] and taking the electrostatic energy at the neutral-solute end to be small (≈0.0), the above surface−bulk difference (+2.4 kcal/mol) corresponds to an electrostatic free-energy difference of ≈1.2 ($=^1/_2 \times 2.4$) kcal/mol, favoring the iodide position in the bulk. However, it must be stressed that the single-iodide-ion system is by no means a true representation of what happens in a NaI solution. The presence of sodium ions and the formation of a double layer may in fact provide further stabilization for the iodide ion at the surface, eventually enhancing the preferential iodide solvation at the surface. In accordance with this, the iodide ions are more

polarized in the NaI solution. The dipole moment components for the two systems are listed in Table 3. In the single-iodide-ion simulations, the average iodide z component is $\langle p_z \rangle = 3.03 \pm 0.6$ D at the surface, compared to 3.40 D in the NaI simulations; similarly, the total average magnitude, $\langle p \rangle$, is 3.42 $\pm$ 0.5 D at the surface, compared to 3.92 D in the NaI solution. The induced dipole moment on water molecules at the first hydration shell of the ion is similar at the bulk (0.66 D) and surface (0.67 D) positions. Note that the iodide polarizes to a significant extent the water molecules at its hydration shell. Indeed, the induced water dipole moment at the surface hydration shell, $\langle p^{WAT} \rangle$, is 0.67 D; in the NaI simulations, the induced water dipole moment (averaged over all of the water molecules at the location of the maximum iodide peak, interface plane $z = 15.0$ Å) was 0.57 D.

The linear-response approximation was used above to provide an estimate of the electrostatic contribution to the free-energy difference between the two positions (i.e., the free energy required to insert an iodide particle at the surface versus the corresponding quantity for the insertion in the bulk); it is not certain to what extent this approximation is valid, especially for the case of introducing a charge at the surface position. Furthermore, the total free-energy difference contains an additional term, equal to the difference in the free energy associated with the introduction of a van der Waals sphere in the two positions. These questions merit a detailed investigation and will be the subject of another publication.

4. Conclusions

Recent computational[19−25] studies based on polarizable models have shown that polarizable ions, such as heavy halides, solvate with a preference for the air−water interface, in agreement with earlier and more recent ion cluster studies.[8−16,18] Modern experimental methods such as vibrational sum-frequency spectroscopy,[29,30] second-harmonic generation,[31,32] and X-ray photoelectron spectroscopy[33] as well as molecular simulations of aqueous sodium iodide vibrational sum-frequency spectra[23] have been used to probe the surfaces of electrolyte solutions.

In the present work, we have examined the solvation of sodium and iodide ions near the water surface, by simulating a 1.2 M NaI solution with a recently developed polarizable water model.[35,36,38,39] In the simulations, the iodide ions are preferentially located at the surface and the sodium ions at an adjacent, interior layer. The double layer arrangement agrees with the theoretical[19,21−23] and experimental[30,33] results. The solvation of sodium near the interface has also been observed in earlier water cluster simulations by Ladanyi and co-workers.[17] Both ionic species and water have nonzero induced dipole moments with a magnitude that depends on the species polarizability and the distance from the interface. In the bulk, the induced dipole moment vectors have a random direction, but near the surface, they are perpendicular to the interface and point toward the air. The water acquires a nonzero permanent dipole moment component in the direction perpendicular to the interface at a depth of 3−5 Å. This subsurface water ordering has also been observed by Tobias and co-workers, who suggested that it contributes to the intensity increase in the sum-frequency spectrum of sodium halide air−water interfaces, with respect to the neat water spectrum.[23]

Additional calculations were conducted with a simpler system, consisting of a single iodide ion in a water slab; this system was chosen in order to illuminate the relative strength of various iodide−water interactions close and away from the air−water interface. Energetic analysis of the simulations showed that the location of iodide at the interface is stabilized by solute−water interactions in which the induced charges play a major role; in contrast, the interactions between the solute and solvent permanent charges favor bulk solvation. Thus, polarizability is essential for the increased preference of iodide for the air−water interface. In the case of sodium ions, the polarizability is very weak and its effect on the stabilization of the interface position is expected to be much smaller. This is in accordance with the sodium profiles, that were evaluated in the NaI simulations.

The surprisingly large contribution of induced dipole moments to the interfacial stabilization is an issue that must be addressed by future theoretical models of the surface tension of electrolyte solutions. It is missing in all current theoretical attempts.[48−50] We are currently continuing this investigation with a more complete thermodynamic analysis of the ionic surface solvation and by considering additional electrolytes.

Acknowledgment. This research was supported by the University of Cyprus. We acknowledge useful discussions with Benoit Roux, Guillaume Lamoureux, and Alexander D. Mackerell. We thank Guillaume Lamoureux and Benoit Roux for providing the ion parameters prior to publication. All simulations were performed on a Linux cluster at the University of Cyprus (UC), that was purchased in part through the programs "DNA oxidative repair by DNA photolyase: Insights from Molecular Dynamics Simulations and Electron Transfer Calculations" (UC) and "Study of Compstatin, important inhibitor of autoimmune system with high accuracy molecular simulations" (RPF/ERYAN/0603) (grants to G.A.).

References and Notes

(1) Collins, K. D.; Washabaugh, M. W. *Q. Rev. Biophys.* **1985**, *18*, 323−422.
(2) Leontidis, E. *Curr. Opin. Colloid Interface Sci.* **2002**, *7*, 81−91.
(3) Baldwin, R. L. *Biophys. J.* **1996**, *71*, 2056−2063.
(4) Ninham, B. W.; Yaminski, V. *Langmuir* **1997**, *13*, 2097−2108.
(5) Kunz, W.; Nostro, P. L.; Ninham, B. W. *Curr. Opin. Colloid Interface Sci.* **2004**, *9*, 1−18.
(6) Weissenhorn, P. K.; Pugh, R. J. *J. Colloid Interface Sci.* **1996**, *184*, 550−563.
(7) Onsager, L.; Samaras, N. N. T. *J. Chem. Phys.* **1934**, *2*, 528−536.
(8) Perera, L.; Berkowitz, M. L. *J. Chem. Phys.* **1991**, *95*, 1954−1963.
(9) Perera, L.; Berkowitz, M. L. *J. Chem. Phys.* **1992**, *96*, 8288−8294.
(10) Perera, L.; Berkowitz, M. L. *J. Chem. Phys.* **1993**, *99*, 4236−4237.
(11) Dang, X. L.; Garrett, B. C. *J. Chem. Phys.* **1993**, *99*, 2972−2977.
(12) Dang, X. L.; Smith, D. E. *J. Chem. Phys.* **1993**, *99*, 6950−6956.
(13) Xantheas, S. *J. Phys. Chem.* **1996**, *100*, 9703−9713.
(14) Stuart, S. J.; Berne, B. J. *J. Phys. Chem.* **1996**, *100*, 11934.
(15) Yeh, I.-C.; Perera, L.; Berkowitz, M. L. *Chem. Phys. Lett.* **1997**, *264*, 31−38.
(16) Stuart, S. J.; Berne, B. J. *J. Phys. Chem. A* **1999**, *103*, 10300.
(17) Perlherbe, G. H.; Ladanyi, B. M.; Hynes, J. T. *Chem. Phys.* **2000**, *258*, 201−224.
(18) Herce, D. H.; Perera, L.; Darden, T. A.; Sagui, C. *J. Chem. Phys.* **2005**, *122*, 024513.
(19) Jungwirth, P.; Tobias, D. J. *J. Phys. Chem. B* **2001**, *105*, 10468−10472.
(20) Dang, X. L.; Chang, T.-M. *J. Phys. Chem. B* **2002**, *106*, 235−238.
(21) Jungwirth, P.; Tobias, D. J. *J. Phys. Chem. B* **2002**, *106*, 6361−6373.
(22) Vrbka, L.; Mucha, M.; Minofar, B.; Jungwirth, P.; Brown, E. C.; Tobias, D. J. *Curr. Opin. Colloid Interface Sci.* **2004**, *9*, 67−73.
(23) Brown, E. C.; Mucha, M.; Jungwirth, P.; Tobias, D. J. *J. Phys. Chem. B* **2005**, *109*, 7934−7940.
(24) Gopalakrishnan, S.; Jungwirth, P.; Tobias, D. J.; Allen, H. C. *J. Phys. Chem. B* **2005**, *109*, 8861−8872.
(25) Brown, E. C.; Mucha, M.; Jungwirth, P.; Tobias, D. J. *J. Phys. Chem. B* **2005**, *109*, 7617−7623.
(26) Markovich, G.; Giniger, R.; Levin, M.; Chesnovsky, O. *J. Chem. Phys.* **1991**, *95*, 9416−9419.
(27) Wilson, M.; Pohorille, A. *J. Chem. Phys.* **1991**, *95*, 6005−6013.

(28) Weber, R.; Winter, B.; Schmidt, P. M.; Widdra, W.; Hertel, I. V.; Dittmar, M.; Faubel, M. *J. Phys. Chem. B* **2004**, *108*, 4729−4736.
(29) Raymond, E. A.; Richmond, G. L. *J. Phys. Chem. B* **2004**, *108*, 5051−5059.
(30) Liu, D.; Ma, G.; Levering, M. L.; Allen, H. C. *J. Phys. Chem. B* **2004**, *108*, 2252−2260.
(31) Petersen, P. B.; Johnson, J. C.; Knutsen, K. P.; Saykally, R. J. *Chem. Phys. Lett.* **2004**, *397*, 46−50.
(32) Petersen, P. B.; Saykally, R. J. *Chem. Phys. Lett.* **2004**, *397*, 51−55.
(33) Ghosal, S.; Hemminger, J.; Bluhm, H.; Mun, B.; Hebenstreit, E. L. D.; Ketteler, G.; Ogletree, D. F.; Requejo, F. G.; Salmeron, M. *Science* **2005**, *307*, 563−566.
(34) Garrett, B. *Science* **2004**, *303*, 1146−1147.
(35) Lamoureux, G.; Mackerell, A. D.; Roux, B. *J. Chem. Phys.* **2003**, *119*, 5185−5197.
(36) Lamoureux, G.; Roux, B. Manuscript to be published.
(37) Lamoureux, G.; Roux, B. *J. Chem. Phys.* **2003**, *119*, 3025−3039.
(38) Noskov, Y. S.; Lamoureux, G.; Roux, B. *J. Phys. Chem. B.*, in press.
(39) Anisimov, V. M.; Lamoureux, G.; Vorobyov, I. V.; Huang, N.; Roux, B.; Mackerell, A. D. *J. Chem. Theory Comput.* **2005**, *1*, 153−168.
(40) Benjamin, I. *J. Chem. Phys.* **1991**, *95*, 3698−3709.
(41) Jungwirth, P.; Tobias, D. J. *J. Phys. Chem. B* **2000**, *104*, 7702−7706.
(42) Brooks, B. R.; Bruccoleri, R. E.; Olafson, B. D.; States, D. J.; Swaminathan, S.; Karplus, M. *J. Comput. Chem.* **1983**, *4*, 187−217.
(43) Darden, T.; York, D.; Pedersen, L. *J. Chem. Phys.* **1993**, *98*, 10089−10092.
(44) Martyna, G.; Tuckerman, M. E.; Tobias, D. J.; Klein, M. L. *Mol. Phys.* **1996**, *87*, 1117.
(45) Martyna, G.; Tobias, D. J.; Klein, M. L. *J. Chem. Phys.* **1994**, *101*, 4177.
(46) Landau, L.; Lifschitz, E. *Electrodynamics of continuous media*; Pergamon Press: New York, 1980.
(47) Archontis, G.; Simonson, T. *Biophys. J.* **2005**, *88*, 3888−3904.
(48) Boström, D.; Williams, D. R. M.; Ninham, B. W. *Langmuir* **2001**, *17*, 4475−4478.
(49) Manciu, M.; Ruckenstein, E. *Adv. Colloid Interface Sci.* **2003**, *105*, 63−101.
(50) Boström, D.; Kunz, D.; Ninham, B. W. *Langmuir* **2005**, *21*, 2619−2623.
(51) Franks, F., Ed. *The Physics and Physical Chemistry of Water*; Water: A Comprehensive Treatise Vol. 1; Plenum Press: New York, 1982.
(52) Mahan, G. D. *Phys. Rev. A* **1980**, *22*, 1780−1785.
(53) Hattig, C.; Hess, A. B. *J. Chem. Phys.* **1998**, *108*, 3863−3870.